



1 **A probabilistic framework for the cover effect in bedrock erosion**

2
3

4 Jens M. Turowski

5 *Helmholtzzentrum Potsdam, German Research Centre for Geosciences GFZ, Telegrafenberg, 14473*
6 *Potsdam, Germany, turowski@gfz-potsdam.de*

7 Rebecca Hodge

8 *Department of Geography, Durham University, Durham, DH1 3LE, United Kingdom,*
9 *rebecca.hodge@durham.ac.uk*

10
11

12 **Abstract**

13 The cover effect in fluvial bedrock erosion is a major control on bedrock channel morphology and long-
14 term channel dynamics. Here, we suggest a probabilistic framework for the description of the cover
15 effect that can be applied to field, laboratory and modelling data and thus allows the comparison of
16 results from different sources. The framework describes the formation of sediment cover as a function
17 of the probability of sediment being deposited on already alleviated areas of the bed. We define
18 benchmark cases and suggest physical interpretations of deviations from these benchmarks.
19 Furthermore, we develop a reach-scale model for sediment transfer in a bedrock channel and use it to
20 clarify the relations between the sediment mass residing on the bed, the exposed bedrock fraction and
21 the transport stage. We derive system time scales and investigate cover response to cyclic
22 perturbations. The model predicts that bedrock channels achieve grade in steady state by adjusting
23 bed cover. Thus, bedrock channels have at least two characteristic time scales of response. Over short
24 time scales, the degree of bed cover is adjusted such that they can just transport the supplied sediment
25 load, while over long time scales, channel morphology evolves such that the bedrock incision rate
26 matches the tectonic uplift or base level lowering rate.

27

28 **1. Introduction**

29

30 Bedrock channels are shaped by erosion caused by countless impacts of the sediment particles they
31 carry along their bed (Beer and Turowski, 2015; Cook et al., 2013; Sklar and Dietrich, 2004). There are
32 feedbacks between the evolving channel morphology, the bedload transport, and the hydraulics
33 (e.g., Finnegan et al., 2007; Johnson and Whipple, 2007; Wohl and Ikeda, 1997). Impacting bedload
34 particles driven forward by the fluid forces erode and therefore shape the bedrock bed. In turn, the
35 morphology of the channel determines the pathways of both sediment and water, and sets the stage
36 for the entrainment and deposition of the sediment (Hodge and Hoey, 2016). Sediment particles play
37 a key role in this erosion process; they provide the tools for erosion and also determine where
38 bedrock is exposed such that it can be worn away by impacting particles (Gilbert, 1877; Sklar and
39 Dietrich, 2004).

40

41 The importance of the cover effect - that a stationary layer of gravel can shield the bedrock from
42 bedload impacts - has by now been firmly established in a number of field and laboratory studies
43 (e.g., Chatanantavet and Parker, 2008; Finnegan et al., 2007; Hobley et al., 2011; Johnson and
44 Whipple, 2007; Turowski and Rickenmann, 2009; Turowski et al., 2008; Yanites et al., 2011).
45 Sediment cover is generally modelled with generic relationships that predict the decrease of the
46 fraction of exposed bedrock area A^* with the increase of the relative sediment supply Q_s^* , usually
47 defined as the ratio of sediment supply to transport capacity. Based on laboratory experiments and
48 simple modeling, Turowski and Bloem (2016) argued that the focus on covered area is generally



49 justified on the reach scale and that erosion of bedrock under a thin sediment cover can be
50 neglected. However, the behavior of sediment cover under flood conditions is currently unknown
51 and the assumption that the cover distribution at low flow is representative for that at high flow may
52 not be justified (cf. Turowski et al., 2008).

53

54 The most commonly used function to describe the cover effect is the linear decline (Sklar and
55 Dietrich, 1998), which is the simplest function connecting the steady state end members of an empty
56 bed when $Q_s^* = 0$ and full cover when $Q_s^* = 1$:

57

$$58 \quad A^* = \begin{cases} 1 - Q_s^* & \text{for } Q_s^* < 1 \\ 0 & \text{otherwise} \end{cases}$$

59 (eq. 1)

60 In contrast, the exponential cover function arises under the assumption that particle deposition is
61 equally likely for each part of the bed, whether it is covered or not (Turowski et al., 2007).

62

$$63 \quad A^* = \begin{cases} \exp(-Q_s^*) & \text{for } Q_s^* < 1 \\ 0 & \text{otherwise} \end{cases}$$

64 (eq. 2)

65 Here, exp denotes the natural exponential function.

66

67 Hodge and Hoey (2012) obtained both the linear and the exponential functions using a cellular
68 automaton (CA) model that modulated grain entrainment probabilities by the number of
69 neighbouring grains. However, consistent with laboratory flume data, the same model also produced
70 other behaviours under different parameterisations. One alternative behavior is runaway alluviation,
71 which was attributed by Chatanantavet and Parker (2008) to the differing roughness of bedrock and
72 alluvial patches. Due to a decrease in flow velocity, an increase in surface roughness and differing
73 grain geometry, the likelihood of deposition is higher over bed sections covered by alluvium
74 compared to bare bedrock sections (Hodge et al., 2011). This can lead to rapid alluviation of the
75 entire bed once a minimum fraction has been covered. The relationship between sediment flux and
76 cover is also affected by the bedrock morphology; flume experiments have demonstrated that on a
77 non-planar bed the location of sediment cover is driven by bed topography and hydraulics (e.g.,
78 Finnegan et al., 2007; Inoue et al., 2014). Johnson and Whipple (2007) found that stable patches of
79 alluvium tended to form in topographic lows such as pot holes and at the bottom of slot canyons,
80 whereas Hodge and Hoey (2016) found that local flow velocity also controls sediment cover location.

81

82 The relationship between roughness, bed cover and incision was explored in a number of recent
83 numerical modeling studies. Nelson and Seminara (2011, 2012) were one of the first to model the
84 impact that the differing roughness of bedrock and alluvial areas has on sediment patch stability.
85 Zhang et al. (2014) formulated a macro-roughness cover model, in which sediment cover is related to
86 the ratio of sediment thickness to bedrock macro-roughness. Aubert et al. (2016) directly simulated
87 the dynamics of particles in a turbulent flow and obtained both linear and exponential cover
88 functions. Johnson (2014) linked erosion and cover to bed roughness in a reach-scale model. Using a
89 model formulation similar to that of Nelson and Seminara (2011), Inoue et al. (2016) reproduced bar
90 formation and sediment dynamics in bedrock channels. All of these studies used slightly different
91 approaches and mathematical formulations to describe alluvial cover, making a direct comparison
92 difficult.

93

94 Over time scales including multiple floods, the variability in sediment supply is also important. Lague
95 (2010) used a model formulation in which cover was written as a function of the average sediment



96 depth to upscale daily incision processes to long time scales. He found that over the long term, cover
97 dynamics are largely independent of the precise formulation at the process scale and are rather
98 controlled by the magnitude-frequency distribution of discharge and sediment supply. Using the CA
99 model of Hodge and Hoey (2012), Hodge (in press) found that, when sediment supply was very
100 variable, sediment cover was primarily determined by the recent history of sediment supply, rather
101 than the relationships identified under constant sediment fluxes.

102

103 So far, it has been somewhat difficult to compare and discuss the different cover functions obtained
104 from theoretical considerations, numerical models, and experiments, since a unifying framework and
105 clear benchmark cases have been missing. Here, we propose such a framework, and develop type
106 cases linked to physical considerations of the flow hydraulics and sediment erosion and deposition.
107 We show how this framework can be applied to data from a published model (Hodge and Hoey,
108 2012). Furthermore, we develop a reach-scale erosion-deposition model that allows the dynamic
109 modeling of cover and prediction of steady states. Thus, we clarify the relationship between cover,
110 deposited mass and relative sediment supply. As part of this model framework we investigate the
111 response time of a channel to a change in sediment input, which we illustrate using data from a
112 natural channel.

113

114 2. A probabilistic framework

115

116 2.1. Development

117 Here we build on the arguments put forward by Turowski et al. (2007) and Turowski (2009). Consider
118 a bedrock bed on which sediment particles are distributed. We can view the deposition of each
119 particle as a random process, and each area element on the bed surface can be assigned a probability
120 for the deposition of a particle. When assuming that a given number of particles are distributed on
121 the bed, the mean behavior of the exposed area can be calculated from the following equation:

$$122 \quad dA^* = -P(A^*, M_s^*, \dots) dM_s^*$$

123 (eq. 3)

124 Here, P is the probability that a given particle is deposited on the exposed part of the bed, which may
125 be a function of the fraction of exposed area, the relative sediment supply, the bed topography and
126 roughness, the particle size, the local hydraulics or other control variables. M_s^* is a dimensionless
127 mass equal to the total mass of the particles residing on the bed per area, which is suitably
128 normalized. A suitable mass for normalization is the minimum mass required to cover a unit area, M_0 ,
129 as will become clear later. The minus sign is introduced because the fraction of the exposed area
130 reduces as M_s^* increases. Similar to eq. (3), the equation for the fraction of covered area $A_c^* = 1 - A^*$
131 can be written as:

132

$$133 \quad dA_c^* = P(A^*, M_s^*, \dots) dM_s^*$$

134 (eq. 4)

135 As most previous relationships are expressed in terms of Q_s^* , the relation of M_s^* to Q_s^* will be
136 discussed later.

137

138 We can make some general statements about P . First, P is defined for the range $0 \leq A^* \leq 1$ and
139 undefined elsewhere. Second, P takes values between zero and one for $0 \leq A^* \leq 1$. Third, $P(A^*=0) = 0$
140 and $P(A^*=1) = 1$. Note that P is not a distribution function and therefore does not need to integrate
141 to one. Neither does it have to be continuous and differentiable everywhere.

142

143 For purpose of illustration, we will next discuss two simple forms of the probability function P that
144 lead to the linear and exponential forms of the cover effect, respectively. First, consider the case that



145 all particles are always deposited on exposed bedrock. In this case, formally, to keep with the
 146 conditions stated above, we define $P = 1$ for $0 < A^* \leq 1$ and $P = 0$ for $A^* = 0$. Thus, we can write
 147

$$148 \quad \begin{aligned} dA^* &= -dM_s^* & \text{for } 0 < A^* \leq 1 \\ dA^* &= 0 & \text{for } A^* = 0 \end{aligned}$$

149 (eq. 5)

150 Integrating, we obtain:

$$151 \quad A^* = -M_s^* + C$$

152 (eq. 6)

153 where the constant of integration C is found to equal one by using the condition $A^*(M_s^*=0) = 1$. Thus,
 154 we obtain the linear cover function of eq. (1). Note that the linear cover function gives a theoretical
 155 lower bound for the amount of cover: it arises when all available sediment always falls on uncovered
 156 ground, and thus no additional sediment is available that could facilitate quicker alluviation. In
 157 essence, this is a mass conservation argument. Now it is obvious why M_0 is a convenient way to
 158 normalize: in plots of A^* against M_s^* , we obtain a triangular region bounded by the points [0,1], [0,0]
 159 and [1,0] in which the cover function cannot run (Fig. 1).
 160

161 Similarly to above, if we set P to a constant value smaller than one for $0 < A^* \leq 1$, k , we obtain
 162

$$163 \quad A^* = 1 - kM_s^*$$

164 (eq. 7)

165 It is clear that the assumption of $P = k$ is physically unrealistic, because it implies that the probability
 166 of deposition on exposed ground is independent of the amount of uncovered bedrock. Especially
 167 when A^* is close to zero, it seems unlikely that, say, always 90% of the sediment falls on uncovered
 168 ground. A more realistic assumption is that the probability of deposition on uncovered ground is
 169 independent of location and other possible controls, but is equal to the fraction of exposed area, i.e.,
 170 $P = A^*$. In a probabilistic sense, this is also the simplest plausible assumption one can make. Then
 171

$$172 \quad dA^* = -A^* dM_s^*$$

173 (eq. 8)

174 giving upon integration

$$175 \quad A^* = e^{-M_s^*}$$

176 (eq. 9)

177 The argument used here to obtain the exponential cover effect in eq. (9) essentially corresponds to
 178 the one given by Turowski et al. (2007). Since this case presents the simplest plausible assumption,
 179 we will use it as a benchmark case, to which we will compare other possible functional forms of P .
 180

181 In principle, the probability function P can be varied to account for various processes that make
 182 deposition more likely either on already covered ground by decreasing P for the appropriate range of
 183 A^* from the benchmark case $P = A^*$, or on uncovered ground by increasing P from the benchmark
 184 case $P = A^*$. As has been identified previously (Chatanantavet and Parker, 2008; Hodge and Hoey
 185 2012), roughness feedbacks to the flow can cause either case depending on whether subsequent
 186 deposition is adjacent to or on top of existing sediment patches. In the former case, particles residing
 187 on an otherwise bare bedrock bed act as obstacles for moving particles, and create a low-velocity
 188 wake zone in the downstream direction. In addition, particles residing on other single particles are
 189 unstable and stacks of particles are unlikely. Hence, newly arriving particles tend to deposit either
 190 upstream or downstream of stationary particles and the probability is generally higher for deposition
 191 on uncovered ground than in the benchmark case. In the latter case, larger patches of stationary
 192 particles increase the surface roughness of the bed, thus decreasing the local flow velocity and



193 stresses, making deposition on the patch more likely. In this way, the probability of deposition on
194 already covered bed is increased in comparison to the benchmark case.

195

196 A simple functional form that can be used to take into account either one of these two effects is a
197 power law dependence of P on A^* , taking the form $P = A^{*\alpha}$ (Fig. 1A). Then, the cover function
198 becomes

199

$$200 \quad A^* = (1 - (1 - \alpha)M_s^*)^{\frac{1}{1-\alpha}}$$

201 (eq. 10)

202 Here, the probability of deposition on uncovered ground is increased in comparison to the
203 benchmark exponential case if $0 < \alpha < 1$, and decreased if $\alpha > 1$.

204

205 A convenient and flexible way to parameterize $P(A^*)$ in general is the cumulative version of the Beta
206 distribution, given by:

$$207 \quad P(A^*) = B(A^*; a, b)$$

208 (eq. 11)

209 Here, $B(A^*; a, b)$ is the regularized incomplete Beta function with two shape parameters a and b ,
210 which are both real positive numbers, defined by:

$$211 \quad B(A^*; a, b) = \frac{\int_0^{A^*} y^{a-1}(1-y)^{b-1} dy}{\int_0^1 y^{a-1}(1-y)^{b-1} dy}$$

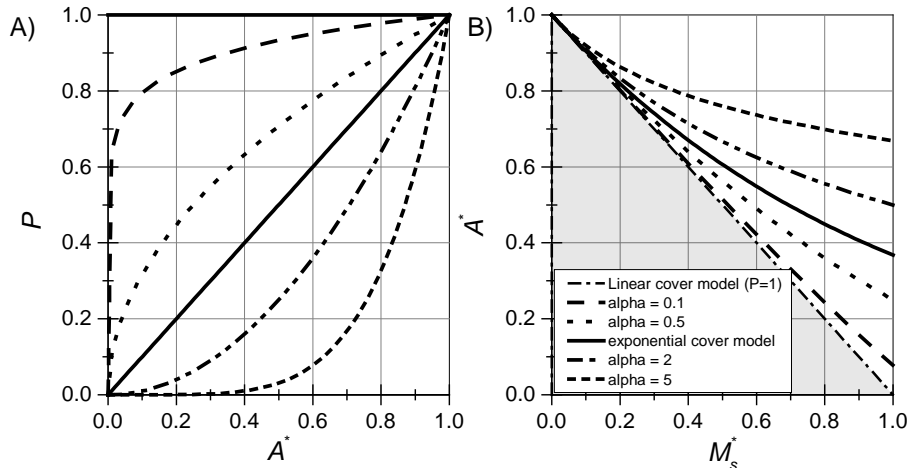
212 (eq. 12)

213 Here, y is a dummy variable. With suitable choices for a and b , cover functions resembling the
214 exponential ($a=b=1$), the linear form ($a=0, b>0$), and the power law form ($a>b$ or $a<b$) can be
215 retrieved. Wavy functions are also a possibility (Fig. 2), thus both of the roughness effects described
216 above can be modelled in a single scenario. Unfortunately, the integral necessary to obtain $A^*(M_s^*)$
217 does not give a closed-form analytical solution and needs to be computed numerically.

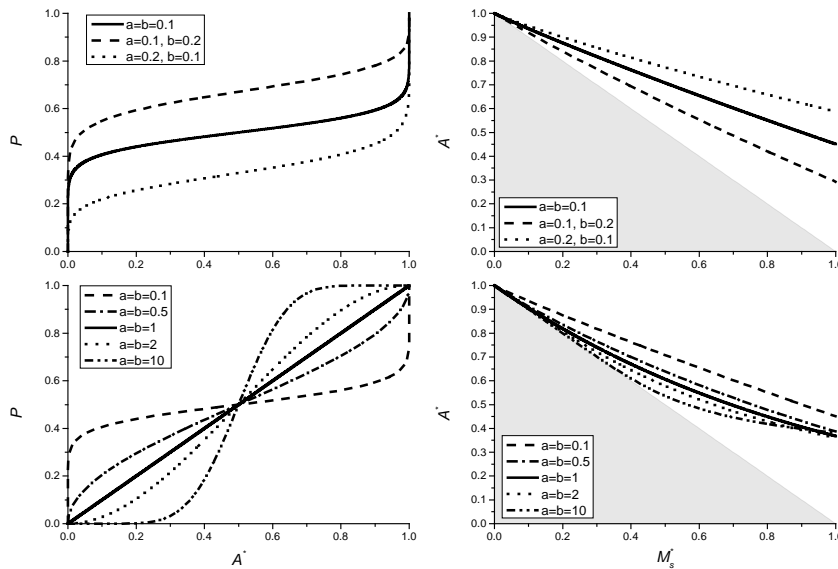
218

219 In principle, a suitable function P could also be defined to account for the influence of bed
220 topography on sediment deposition. Such a function is likely dependent on the details of the
221 particular bed, hydraulics and sediment flow paths in a complex way and needs to be mapped out
222 experimentally.

223



224
 225 Fig. 1: A) Various examples for the probability function P as a function of bedrock exposure A^* . B)
 226 Corresponding analytical solutions for the cover function between A^* and dimensionless sediment
 227 mass M_s^* using eq. (7), (9) and (10). Grey shading depicts the area where the cover function
 228 cannot run due to conservation of mass.
 229



230
 231 Fig. 2: Examples for the use of the regularized incomplete Beta function (eq. 12) to parameterize P ,
 232 using various values for the shape parameters a and b . The choice $a = b = 1$ gives a dependence that
 233 is equivalent to the exponential cover function. Grey shading depicts the area where the cover
 234 function cannot run due to conservation of mass.
 235



236 2.2 Example of application using model data

237

238 To illustrate how the framework can be used, we apply it to data obtained from the CA model
239 developed by Hodge and Hoey (2012). The CA model reproduces the transport of individual sediment
240 grains over a bedrock surface. In each time step, the probability of a grain being entrained is a
241 function of the number of neighboring grains. If five or more of the eight neighbouring cells contain
242 grains then the grain has probability of entrainment P_c , otherwise it has probability P_i . In most model
243 runs P_c is less than P_i , thus accounting for the impact of sediment cover in decreasing local shear
244 stress (though increased flow resistance) and increasing the critical entrainment shear stress for
245 grains (via lower grain exposure and increased pivot angles).

246

247 The model is run with a domain that is 100 cells wide by 1000 cells long, with each cell having the
248 same area as a grain. Up to four grains can potentially be entrained from each cell in a time step,
249 limiting the maximum sediment flux. In each time step random numbers and the probabilities are
250 used to select the grains that are entrained, which are then moved a step length downstream. A
251 fixed number of grains are also supplied to the upstream end of the model domain. A smoothing
252 algorithm is applied to prevent local excessively tall piles of grains. After around 500 time steps the
253 model typically reaches a steady state condition in which the number of grains supplied to and
254 leaving the model domain are equal. Sediment cover is measured in a downstream area of the model
255 domain and is defined as grains that are not entrained in a given time step.

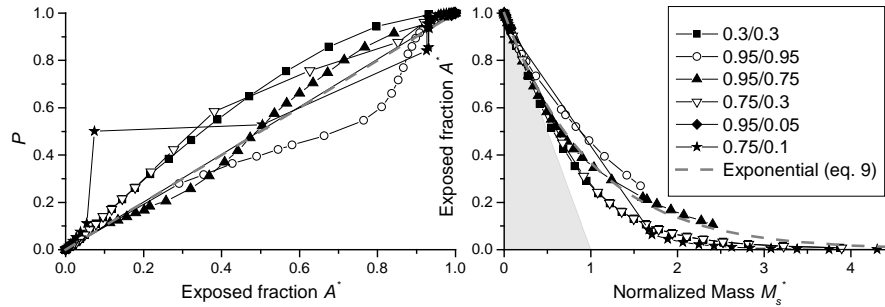
256

257 Model runs were completed with a six different combinations of P_i and P_c : 0.95/0.95, 0.95/0.75,
258 0.75/0.10, 0.75/0.30, 0.30/0.30 and 0.95/0.05. These combinations were selected to cover the range
259 of relationships between Q_s^* and A_c^* observed by Hodge and Hoey (2012). For each pair of P_i and P_c
260 model runs were completed at least 20 different values of Q_s^* in order to quantify the model
261 behaviour.

262

263 Cover bed fraction and total mass on the bed given out by the model were converted using eq. (3)
264 into the probabilistic framework (Fig. 3). The derivative was approximated by simple linear finite
265 differences, which, in the case of run-away alluviation, resulted in a non-continuous curve due to
266 large gradients. The exponential benchmark (eq. 9) is also shown for comparison. The different
267 model parameterisations produce results in which the probability of deposition on bedrock is both
268 more and less likely than in the baseline case, with some runs showing both behaviours. Cases where
269 the probability is more than the baseline case (i.e. grains are more likely to fall on uncovered areas)
270 are associated with runs in which grains in clusters are relatively immobile. These runs are likely to be
271 particularly affected by the smoothing algorithm that acts to move sediment from alluviated to
272 bedrock areas. All model parameterisations predict greater bed exposure for a given normalised
273 mass than is predicted by a linear cover relationship (Figure 3b). Runs with relatively more immobile
274 cluster grains have a lower exposed fraction for the same normalised mass. Runs with low values of
275 P_i and P_c seem to lead to behavior in which cover is more likely than in the exponential benchmark,
276 while for high values, it is less likely. However, there are complex interactions and general
277 statements cannot be made straightforwardly.

278



279
 280 Fig. 3: Probability functions P and cover function derived from data obtained from the model of
 281 Hodge and Hoey (2012). The grey dashed line shows the exponential benchmark behavior. Grey
 282 shading depicts the area where the cover function cannot run due to conservation of mass. The
 283 legend gives values of P_i and P_c used for the runs (see text).

284

285

3. Cover development in time and space

286

3.1. Model derivation

287

288

289

290

291

292

293

294

295

296

297

298

299

300

301

302

303

304

305

306

307

308

309

310

311

312

313

314

315

316

The probabilistic formulation introduced above can be extended to allow the calculation of the temporal and spatial evolution of sediment cover in a stream. Here, we will derive the equations for the one dimensional case (linear flume), but extensions to higher dimensions are possible in principle. The derivation is inspired by the erosion-deposition framework (e.g. Charru et al., 2004), with some necessary adaptations to make it suitable for channels with partial sediment cover. In our system, we consider two separate mass reservoirs within a control volume. The first reservoir contains all particles in motion, the total mass per bed area of which is denoted by M_m , while the second reservoir contains all particles that are stationary on the bed, the total mass per bed area of which is denoted by M_s . We need then three further equations, one to connect the rate of change of mobile mass to the sediment flux in the flume, one to govern the exchange of particles between the two reservoirs, and one to describe how sediment transport rate is related to the mobile mass. The first of these is of course the Exner equation of sediment continuity (e.g. Paola and Voller, 2005), which captures mass conservation in the system. Instead of the common approach tracking the height of the sediment over a reference level, we use the total sediment mass on the bed as a variable, giving

$$\frac{\partial M_m}{\partial t} = -\frac{\partial q_s}{\partial x} + E - D$$

(eq. 13)

Here, x is the coordinate in the streamwise direction, t the time, q_s the sediment mass transport rate per unit width, while E is the mass entrainment rate per bed area and D is the mass deposition rate per bed area. It is clear that for the problem at hand the choice of total mass or volume as a variable to track the amount of sediment in the reach of interest is preferable to the height of the alluvial cover, since necessarily, when cover is patchy, the height of the alluvium varies across the bed. It is useful to work with dimensionless variables by defining $t^* = t/T$ and $x^* = x/L$, where T and L are suitable time and length scales, respectively. The dimensionless mobile mass per bed area M_m^* is equal to M_m/M_0 , and eq. (13) becomes:



317
$$\frac{\partial M_m^*}{\partial t^*} = -\frac{\partial q_s^*}{\partial x^*} + E^* - D^*$$

318 (eq. 14)

319 Here,

320
$$q_s^* = \frac{T}{LM_0} q_s$$

321 (eq. 15)

322 The dimensionless entrainment and deposition rates, E^* and D^* , are equal to TE/M_0 and TD/M_0 ,
 323 respectively. The rate of change of the stationary sediment mass M_s in time is the difference of the
 324 deposition rate D and the entrainment rate E .

325

326
$$\frac{\partial M_s}{\partial t} = D - E$$

327 (eq. 16)

328 Or, using dimensionless variables

329
$$\frac{\partial M_s^*}{\partial t^*} = D^* - E^*$$

330 (eq. 17)

331 We also need sediment entrainment and deposition functions. The entrainment rate needs to be
 332 modulated by the availability of sediment on the bed. If M_s^* is equal to zero, no material can be
 333 entrained. A plausible assumption is that the maximal entrainment rate, E_{max}^* , is equal to the
 334 transport capacity.

335
$$E_{max}^* = q_t^*$$

336 (eq. 18)

337 Here, q_t^* is the dimensionless mass transport capacity, which is related to the transport capacity per
 338 unit width q_t by a relation similar to eq. (15). To first order, the rate of change in entrainment rate,
 339 dE , is proportional to the difference of E_{max} and E , and to the rate of change in mass on the bed.

340

341
$$dE^* = (E_{max}^* - E^*)dM_s^* = (q_t^* - E^*)dM_s^*$$

342 (eq. 19)

343 Integrating, we obtain

344

345
$$E^* = E_{max}^*(1 - e^{-M_s^*}) = (1 - e^{-M_s^*})q_t^*$$

346 (eq. 20)

347 Here, we used the condition $E^*(0) = 0$ to fix the integration constant to E_{max}^* . As required, eq. (20)
 348 approaches E_{max}^* as M_s^* goes to infinity, and is equal to zero when M_s^* is equal to zero. Using a similar
 349 line of argument, and by assuming the maximum deposition rate to be equal to q_s^* , we arrive at an
 350 equation for the deposition rate D^* .

351

352
$$D^* = (1 - e^{-M_m^*})q_s^*$$

353 (eq. 21)

354 Substituting eqs. (20) and (21) into eq. (17), we obtain:

355

356
$$\frac{\partial M_s^*(x^*, t^*)}{\partial t^*} = D^* - E^* = (1 - e^{-M_m^*(x^*, t^*)})q_s^*(x^*, t^*) - (1 - e^{-M_s^*(x^*, t^*)})q_t^*(x^*, t^*)$$

357 (eq. 22)

358 Note that $q_s^*/q_t^* = Q_s^*$. The equation for the mobile mass (eq. 14) becomes:

359



$$\frac{\partial M_m^*(x^*, t^*)}{\partial t^*} = -\frac{\partial q_s^*}{\partial x^*} - (1 - e^{-M_m^*(x^*, t^*)})q_s^*(x^*, t^*) + (1 - e^{-M_s^*(x^*, t^*)})q_t^*(x^*, t^*)$$

360 (eq. 23)

362 Finally, the sediment transport rate needs to be proportional to the mobile sediment mass times the
 363 downstream sediment speed U , and we can write

$$q_s^*(x^*, t^*) = U^*(x^*, t^*)M_m^*(x^*, t^*)$$

364 (eq. 24)

365 Here

$$U^* = \frac{T}{L}U$$

366 (eq. 25)

367

371 After incorporating the original equation between A^* and M_s^* (eq. 3), the system of four differential
 372 equations (3), (22), (23) and (24) contains four unknowns: the downstream gradient in the sediment
 373 transport rate $\partial q_s^*/\partial x^*$, the exposed fraction of the bed A^* , the non-dimensional stationary mass M_s^* ,
 374 and the non-dimensional mobile mass M_m^* , while the non-dimensional transport capacity q_t^* and the
 375 non-dimensional downstream sediment speed U^* are input variables, and P is an externally specified
 376 function. In addition, sediment input needs to be specified as an upstream boundary condition and
 377 initial values for the mobile and stationary masses need to be specified everywhere.

378

3.2. Time-independent solution

379

381 Setting the time derivatives to zero, we obtain a time-independent solution, which links the exposed
 382 area directly to the ratio of sediment transport rate to transport capacity. From eq. (23) it follows
 383 that in this case, the entrainment rate is equal to the deposition rate and we obtain

$$(1 - e^{-\bar{M}_m^*})\bar{q}_s^* = (1 - e^{-\bar{M}_s^*})\bar{q}_t^*$$

384 (eq. 26)

385 Here, the bar over the variables denotes their steady state value. Substituting eq. (24) to eliminate
 386 \bar{M}_m^* and solving for \bar{M}_s^* gives

387

$$\bar{M}_s^* = -\ln \left\{ 1 - \left(1 - e^{-\bar{q}_s^*/U^*} \right) \frac{\bar{q}_s^*}{\bar{q}_t^*} \right\} = -\ln \left\{ 1 - \left(1 - e^{-\frac{\bar{q}_s^*}{U^* \bar{Q}_s^*}} \right) \bar{Q}_s^* \right\}$$

388 (eq. 27)

391 Note that we assume here that sediment cover is only dependent on the stationary sediment mass
 392 on the bed and we thus neglect grain-grain interactions known as the dynamic cover (Turowski et al.,
 393 2007). In analogy to eq. (24), we can write

$$q_t^* = U^*M_0^*$$

394 (eq. 28)

395 Here, M_0^* is a characteristic dimensionless mass that depends on hydraulics and therefore implicitly
 396 on transport capacity (which is independent of and should not be confused with the minimum mass
 397 necessary to fully cover the bed M_0). When sediment transport rate equals transport capacity, then
 398 M_0^* is equal to the mobile mass of sediment normalized by the reference mass M_0 . It can be viewed
 399 as a proxy for the transport capacity and is a convenient parameter to simplify the equations. The
 400 mobile mass can then, in general, be written as (cf. Turowski et al., 2007), remembering that $Q_s^* = 1$
 401 when transport is equal to capacity:

$$M_m^* = M_0^*Q_s^*$$

402 (eq. 29)



405 If we use the exponential cover function (eq. 9) with eqs. (27), (28) and (29) we obtain
 406

$$407 \quad \bar{A}^* = 1 - \left(1 - e^{-\frac{q_s^*}{u^*}}\right) \frac{q_s^*}{q_t^*} = 1 - \left(1 - e^{-\frac{q_s^*}{u^* Q_s^*}}\right) Q_s^* = 1 - \left(1 - e^{-M_0^* Q_s^*}\right) Q_s^*$$

408 (eq. 30)

409 Similarly, equations can be found for the other analytical solutions of the cover function. For the
 410 linear case (eq. 7), we obtain:

$$411 \quad \bar{A}^* = 1 + \ln\left\{1 - \left(1 - e^{-M_0^* Q_s^*}\right) Q_s^*\right\}$$

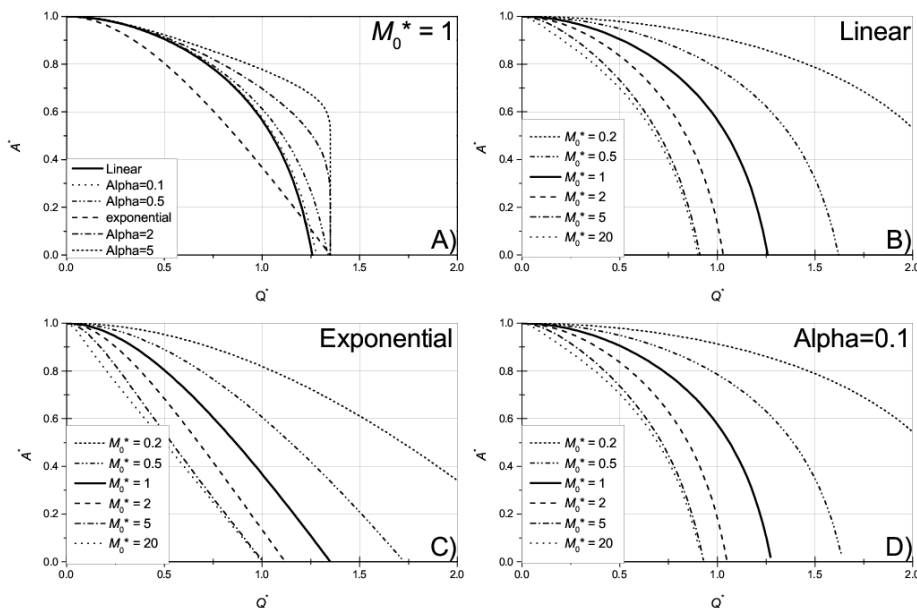
412 (eq. 31)

413 For the power law case (eq. 10), we obtain:

$$414 \quad \bar{A}^* = \left[1 + (1 - \alpha) \ln\left\{1 - \left(1 - e^{-M_0^* Q_s^*}\right) Q_s^*\right\}\right]^{\frac{1}{1-\alpha}}$$

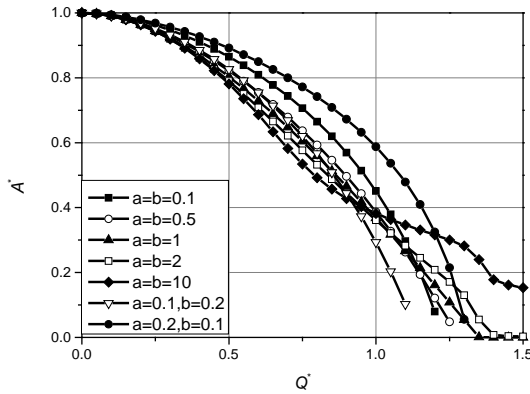
415 (eq. 32)

416 It is interesting that the assumption of an exponential cover function essentially leads to a combined
 417 linear and exponential relation between \bar{A}^* and Q_s^* . Instead of a linear decline as the original linear
 418 cover model, or a concave-up relationship as the original exponential model, the function is convex-
 419 up for all solutions (Fig. 4). Adjusting M_0^* shifts the lines: decreasing M_0^* leads to a delayed onset of
 420 cover and vice versa. The former result arises because a lower M_0^* means that the sediment flux is
 421 conveyed through a smaller mass moving at a higher velocity. The original linear cover function (eq.
 422 1) can be recovered from the exponential model with a high value of M_0^* , since the exponential term
 423 quickly becomes negligible with increasing Q_s^* and the linear term dominates (Fig. 4C). Note that for
 424 the linear (eq. 6) and the power law cases (eq. 10), high values of M_0^* may give $\bar{A}^* = 0$ for $Q_s^* < 1$ (Fig.
 425 4B,D), which is consistent with the concept of runaway alluviation. Using the beta distribution to
 426 describe P , a numerical solution is necessary, but a wide range of steady-state cover functions can be
 427 obtained (Fig. 5). By varying the value of M_0^* , an even wider range of behavior can be obtained.





429 Fig. 4: Analytical solutions at steady state for the exposed fraction of the bed (A^*) as a function of
 430 relative sediment supply (Q^* , cf. Fig. 1). A) Comparison of the different solutions, keeping M_0^*
 431 constant at 1. B) Varying M_0^* for the linear case (eq. 31). C) Varying M_0^* for the exponential case (eq.
 432 30). D) Varying M_0^* for the power law case with $\alpha = 0.1$ (eq. 32).
 433



434 Fig. 5: Steady state solutions using the beta distribution to parameterize P (eq. 11) for a range of
 435 parameters a and b , and using $M_0^* = 1$ (cf. Fig. 2). The solutions were obtained by iterating the
 436 equations to a steady state, using initial conditions of $A^* = 1$ and $M_m^* = M_s^* = 0$.
 437

438
 439 The previous analysis shows that steady state cover is controlled by the characteristic dimensionless
 440 mass M_0^* , which is equal to the ratio of dimensionless transport capacity and particle speed (eq. 28).
 441 Converting to dimensional variables, we can write

$$M_0^* = \frac{q_t^*}{U^*} = \frac{q_t}{M_0 U}$$

442 (eq. 33)

443 The minimum mass necessary to completely cover the bed per unit area, M_0 , can be estimated
 444 assuming a single layer of close-packed spherical grains residing on the bed (cf. Turowski, 2009),
 445 giving:

$$M_0 = \frac{\pi \rho_s D_{50}}{3\sqrt{3}}$$

446 (eq. 34)

447 Here, ρ_s is the sediment density and D_{50} is the median grain size. Fernandez-Luque and van Beek
 448 (1976) derived equations both for the transport capacity and the particle speed from flume
 449 experiments, using bed shear stress as a control parameter (see also Lajeunesse et al., 2010 and
 450 Meyer-Peter and Mueller, 1948 for similar equations).
 451

$$q_t = 5.7 \frac{\rho_s \rho}{(\rho_s - \rho) g} \left(\frac{\tau}{\rho} - \frac{\tau_c}{\rho} \right)^{3/2}$$

452 (eq. 35)

453

$$U = 11.5 \left(\left(\frac{\tau}{\rho} \right)^{1/2} - 0.7 \left(\frac{\tau_c}{\rho} \right)^{1/2} \right)$$

454 (eq. 36)

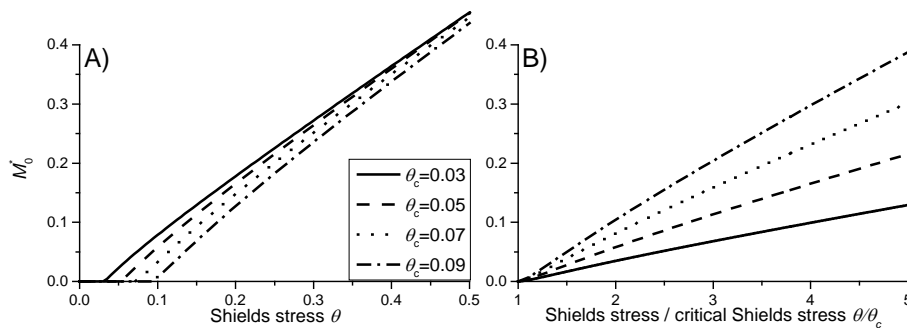


459 Here, τ_c is the critical bed shear stress for the onset of bedload motion, g is the acceleration due to
 460 gravity and ρ is the water density. Combining eqs. (34), (35) and (36) to get an equation for M_0^* gives:
 461

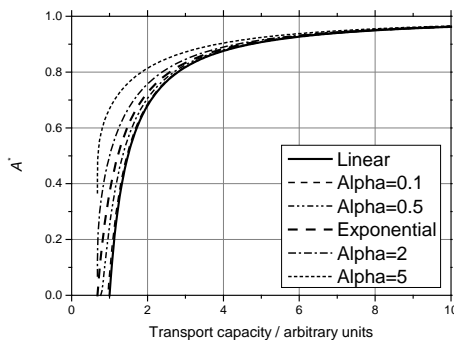
$$462 \quad M_0^* = \frac{3\sqrt{3}}{2\pi} \frac{(\theta - \theta_c)^{3/2}}{\theta^{1/2} - 0.7\theta_c^{1/2}} = \frac{3\sqrt{3}\theta_c}{2\pi} \frac{(\theta/\theta_c - 1)^{3/2}}{(\theta/\theta_c)^{1/2} - 0.7}$$

463 (eq. 37)

464 Here, the Shields stress $\theta = \tau/(\rho_s - \rho)gD_{50}$, and θ_c is the corresponding critical Shields stress, and we
 465 approximated $5.7/11.5 = 0.496$ with $1/2$. At high θ , when the threshold can be neglected, eq. (37)
 466 reduces to a linear relationship between M_0^* and θ . Near the threshold, M_0^* is shifted to lower values
 467 as θ_c increases (Fig. 6). The systematic variation of U^* with the hydraulic driving conditions (eq. 36)
 468 implies that the cover function evolves differently in response to changes in sediment supply and
 469 transport capacity. For a first impression, by comparing equations (35) and (36), we assume that
 470 particle speed scales with transport capacity raised to the power of one third (Fig. 7).
 471



472
 473 Fig. 6: The characteristic dimensionless mass M_0^* depicted as a function of A) the Shields stress and
 474 B) the ratio of Shields stress to critical Shields stress (eq. 37).
 475



476
 477 Fig. 7: Variation of the exposed bed fraction as a function of transport capacity, assuming that
 478 particle speed scales with transport capacity to the power of one third.
 479

480 3.3 Temporal evolution of cover within a reach

481 3.3.1 System timescales

482 To calculate the temporal evolution of cover on the bed within a single reach, we solved the
 483 equations numerically for a section of the bed with homogenous conditions using a simple linear
 484 finite difference scheme. Then, the sediment input is a boundary condition, while sediment output,



485 mobile and stationary sediment mass and the fraction of cover are output variables. In general, a
 486 change in sediment supply leads to a gradual adjustment of the output variables towards a new
 487 steady state (Fig. 8). Unfortunately, a general analytical solution is not possible, but a results can be
 488 obtained for the special case of $q_s^* = 0$. Such a situation is rare in nature, but could be easily created
 489 in flume experiments as a model test. Then, the time derivative of stationary mass is given by:

$$\frac{\partial M_s^*}{\partial t^*} = -(1 - e^{-M_s^*})q_t^*$$

492 (eq. 38)

493 Using the exponential cover model (eq. 9), we obtain:

$$\frac{1}{A^*(1 - A^*)} \frac{\partial A^*}{\partial t^*} = q_t^*$$

496 (eq. 39)

497 Equation (39) is separable and can be integrated to obtain

$$\ln(A^*) - \ln(1 - A^*) = t^* q_t^* + C$$

500 (eq. 40)

501 Letting $A^*(t^*=0) = A_0^*$, where A_0^* is the initial cover, the final equation is

$$\frac{1 - A^* A_0^*}{1 - A_0^* A^*} = e^{-t^* q_t^*}$$

504 (eq. 41)

505 To clarify the characteristic time scale of the process, equation (41) can also be written in the form of
 506 a sigmoidal-type function:

$$A^* = \frac{1}{1 + \left(\frac{1 - A_0^*}{A_0^*}\right) e^{-t^* q_t^*}}$$

509 (eq. 42)

510 By making the parameters in the exponent on the right hand side of eq. (42) dimensional, we get:

$$t^* q_t^* = \frac{t}{T} \frac{T}{LM_0} q_t = \frac{t q_t}{LM_0}$$

513 (eq. 43)

514 which allows a characteristic system time scale T_E to be defined as

$$T_E = \frac{LM_0}{q_t}$$

516 (eq. 44)

517 Since this time scale is dependent on the transport capacity q_t , we can view it as a time scale
 518 associated with the entrainment of sediment from the bed (cf. eq. 20) – hence the subscript E on T_E .
 519 From eq. (42), the exposed bed fraction evolves in an asymptotic fashion towards equilibrium (Fig. 9).
 520 We can expect that there are other characteristic time scales for the system, for example associated
 521 with sediment deposition or downstream sediment evacuation.

522

523 We can make some further progress and define a more general system time scale by performing a
 524 perturbation analysis (Appendix A). For small perturbations in either q_s^* or q_t^* , we obtain an
 525 exponential term describing the transient evolution, which allows the definition of a system
 526 timescale T_S



527
$$\exp\left\{-\left(\frac{\bar{q}_t^*}{\bar{q}_t} - \left(1 - e^{-\frac{\bar{q}_s^*}{U^*}}\right)\frac{\bar{q}_s^*}{\bar{q}_t}\right)t^*\right\} = \exp\left\{-\frac{t}{T_S}\right\}$$

528 (eq. 45)

529 The characteristic system time scale can then be written as

530
$$T_S = \frac{LM_0}{\bar{q}_t \left(1 - \left(1 - e^{-\frac{\bar{q}_s^*}{U^*}}\right)\frac{\bar{q}_s^*}{\bar{q}_t}\right)} = \frac{LM_0}{\bar{q}_t} e^{\bar{M}_s^*}$$

531 (eq. 46)

532 Note that for $q_s^* = 0$, eq. (46) reduces to eq. (44), as would be expected. Since \bar{M}_s^* is directly related
 533 to steady state bed exposure \bar{A}^* , we can rewrite the equation, for example by assuming the
 534 exponential cover function (eq. 3), as

535
$$T_S = \frac{LM_0}{\bar{q}_t \bar{A}^*}$$

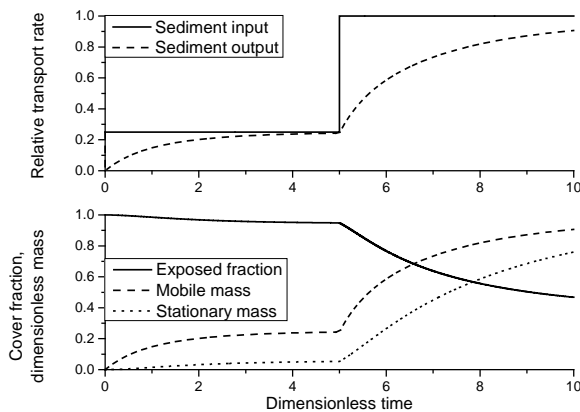
536 (eq. 47)

537 Since bed cover is more easily measurable than the mass on the bed, eq. (47) can help to estimate
 538 system time scales in the field. Further, \bar{A}^* varies between 0 and 1, which allows estimating a
 539 minimum system time using eq. (44). As \bar{A}^* approaches zero, the system time diverges.

540

541 To illustrate these additional dependencies, we have calculated the time need to reach 99.9%
 542 (chosen due to the asymptotic behavior of the system) of total adjustment after a step change in
 543 transport stage, produced by varying particle speed U over a range of plausible values (Fig. 10).
 544 Response time decreases as particle speed increases. This reflects elevated downstream evacuation
 545 for higher particles speeds, resulting in a smaller mobile particle mass and thus higher entrainment
 546 and lower deposition rates. Response time also increases with increasing q_s/q_t . As the runs start with
 547 zero sediment cover, and the extent of cover increases with q_s/q_t , at higher q_s/q_t the adjusted cover
 548 takes longer to develop.

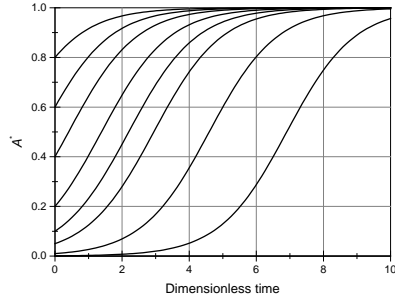
549



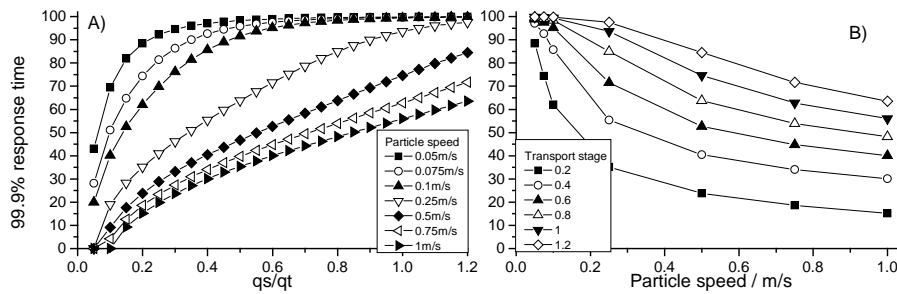
550

551 Fig. 8: Temporal evolution of cover for a simple case. Here, we used the exponential function for P
 552 (eq. 9) and $M_0^* = 1$. The initial values were $A^* = 1$, $M_m^* = M_s^* = 0$ and $q_s^* = 0.25$. Sediment supply was
 553 increased to $q_s^* = 1$ at $t^* = 5$.

554



555
 556 Fig. 9: Evolution of the exposed bed fraction (removal of sediment cover) over time starting with
 557 different initial values of bed exposure, for the special case $q_s^* = 0$ (eq. 41) and $q_i^* = 1$.
 558



559
 560 Fig. 10: Dimensionless time to reach 99.9% of the total adjustment in exposed area as a function of
 561 A) transport stage and B) particle speed. All simulation were started with $A^* = 1$ and $M_m^* = M_s^* = 0$.
 562
 563
 564

565 3.3.2 Phase shift and gain in response to a cyclic perturbation

566 The perturbation analysis (Appendix A) gives some insight into the response of cover to cyclic
 567 sinusoidal perturbations. Let sediment supply be perturbed in a cyclic way described by an equation
 568 of the form

$$569 \quad q_s^* = \overline{q_s^*} + \delta q_s^* = \overline{q_s^*} + d \sin\left(\frac{2\pi t}{p}\right)$$

570 (eq. 48)

571 Here, the overbar denotes the temporal average, δq_s^* is the time-dependent perturbation, d is the
 572 amplitude of the perturbation and p its period. A similar perturbation can be applied to the transport
 573 capacity (see Appendix A). The reaction of the stationary mass and therefore cover can then also be
 574 described by sinusoidal function of the form (Appendix A)

$$575 \quad \delta M_s^* = G \sin\left(\frac{2\pi t}{p} + \varphi\right)$$

576 (eq. 49)

577 Here, δM_s^* is the perturbation of the stationary sediment mass around the temporal average, G is
 578 known as the gain, describing the amplitude response, and φ is the phase shift. If the gain is large,
 579 stationary mass reacts strongly to the perturbation; if it is small, the forcing does not leave a signal.
 580 The phase shift is negative if the response lags behind the forcing and positive if it leads. The phase
 581 shift can be written as



582
$$\varphi = \tan^{-1}\left(-2\pi\frac{T_s}{p}\right)$$

583 (eq. 50)

584 The gain can be written as

585
$$G = \frac{p}{T_s} \frac{Kd}{\sqrt{\left(\frac{p}{T_s}\right)^2 + 4\pi^2}}$$

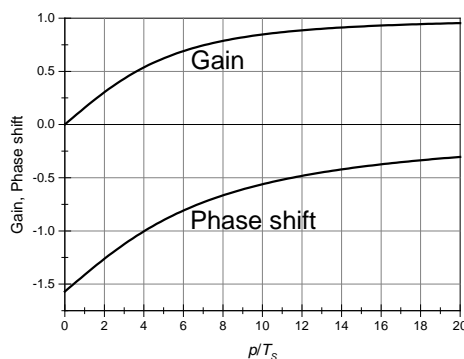
586 (eq. 51)

587 Here, d is the amplitude of the perturbation, and K is a function of the time-averaged values of q_s , q_t
588 and U and differs for perturbations in transport capacity and sediment supply (see Appendix A).

589 Thus, the system behavior can be interpreted as a function of the ratio of the period of perturbation
590 p and the system time scale T_s . The period p is large if the forcing parameter, i.e., discharge or
591 sediment supply, varies slowly and small when it varies quickly. According to eq. (50), the phase shift
592 is equal to $-\pi/2$ for low values of p/T_s (quickly-varying forcing parameter), implying a substantial lag in
593 the adjustment of cover. The phase shift tends to zero as p tends to infinity (Fig. 11). The gain varies
594 approximately linearly with p/T_s for small p/T_s (quickly-varying forcing parameter), while it is
595 approximately constant at a value of Kd for large p/T_s (slowly-varying forcing parameter) (eq. 51).

596 Thus, if the forcing parameter varies slowly, cover adjustment keeps up at all times.

597



598

599 Fig. 11: Phase shift (eq. 50) and gain (eq. 51) as a function of the ratio of the period of perturbation
600 period p and the system time scale T_s . For the calculation, the constant factor in the gain (Kd) was set
601 equal to one.

602

603 3.3.3 A flood at the Erlenbach

604 To illustrate the magnitude of the timescales using real data, we use a flood dataset from the
605 Erlenbach, a sediment transport observatory in the Swiss Prealps (e.g., Beer et al., 2015). There, near
606 a discharge gauge, bedload transport rates are measured at 1-minute resolution using the Swiss Plate
607 Geophone System, a highly developed and fully calibrated surrogate bedload measuring system (e.g.,
608 Rickenmann et al., 2012; Wyss et al. 2016). We use data from a flood on 20th June 2007 (Turowski et
609 al., 2009) with highest peak discharge that has so far been observed at the Erlenbach. The
610 meteorological conditions that triggered this flood and its geomorphic effects have been described in
611 detail elsewhere (Molnar et al., 2010; Turowski et al., 2009). Although the Erlenbach does not have a
612 bedrock bed in the sense that bedrock is exposed in the channel bed, the data provide a realistic
613 natural time series of discharge and bedload transport over the course of a single event and are ideal
614 for illustrating possible cover behavior.

615



616 Using a median grain size of 80 mm, a sediment density of 2650 kg/m³ and a reach length of 50 m,
617 we obtained $M_0 = 128 \text{ kg/m}^2$. We calculated transport capacity using the equation of Fernandez
618 Luque and van Beek (1976). However, it is known that this and similar equations strongly
619 overestimate measured transport rates in streams such as the Erlenbach (e.g., Nitsche et al., 2011).
620 Consequently, we rescaled by setting the ratio of bedload supply to capacity to one at the highest
621 discharge. The exposed fraction was then calculated iteratively assuming $P = A^*$ (i.e., the exponential
622 cover formulation). To estimate the period p , one needs to take the derivatives of eq. (48).

$$623 \quad \frac{dq_s^*}{dt} = \frac{d\delta q_s^*}{dt} = \frac{2\pi d}{p} \cos\left(\frac{2\pi t}{p}\right)$$

624 (eq. 52)

625 Setting $t = 0$ for the time of interest, we can relate p to the local gradient in bedload supply, which
626 can be measured from the data.

627

$$628 \quad \frac{2\pi d}{p} = \frac{\Delta q_s^*}{\Delta t}$$

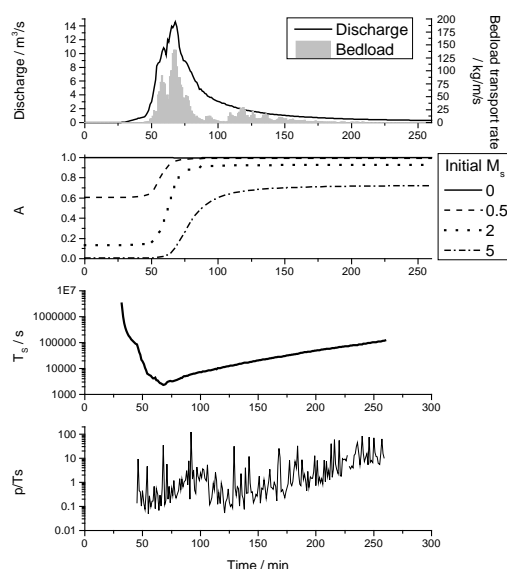
629 (eq. 52)

630 Assuming that all change in the response time is due to changes in the period (i.e., assuming constant
631 amplitude, $d = 1$), we can obtain a conservative estimate of the range over which p varies over the
632 course of an event.

$$633 \quad p = 2\pi \frac{\Delta t}{\Delta q_s^*}$$

634 (eq. 52)

635 In the exemplary event, the evolution and final value of bed cover depends strongly on its initial
636 value (Fig. 12), indicating that the adjustment is incomplete. The system timescale is generally larger
637 than 1000s and is inversely related to discharge via the dependence on transport capacity. The
638 p/T_s ratio varies around one, with low values at the beginning of the flood and large values in the
639 waning hydrograph. Both the high system times and the smooth evolution of bed cover over the
640 course of the flood imply that cover development cannot keep up with the variation in the forcing
641 characteristics. This dynamic adjustment of cover, which can lag forcing processes, may thus play an
642 important role in the dynamics of bedrock channels and probably needs to be taken into account in
643 modelling exercises.



644
645 Fig. 12: Calculated evolution of cover during the largest event observed at the Erlenbach on 20th June
646 2007 (Turowski et al., 2009). Bedload transport rates were measured with the Swiss Plate geophone
647 sensors calibrated with direct bedload samples (Rickenmann et al., 2012). The final fraction of
648 exposed bedrock is strongly dependent on its initial value.

649

650 4. Discussion

651

651 4.1 Model formulation

652

653 In principle, the framework for the cover effect presented here allows the formulation of a general
654 model for bedrock channel morphodynamics without the restrictions of previous models (e.g. Zhang
655 et al., 2015). To achieve this, the dependency of P on various control parameters needs to be
656 specified. In general, P should be controlled by local topography, grain size and shape, hydraulic
657 forcing, and the amount of sediment already residing on the bed. Furthermore, the shape of the P
658 function should also be affected by feedbacks between these properties, such as the development of
659 sediment cover altering the local roughness and hence altering hydraulics and local transport
660 capacity (Inoue et al., 2014; Johnson, 2014). Within the treatment presented here, we have explicitly
661 accounted only for the impact of the amount of sediment already on the bed. However, all of the
662 mentioned effects can be included implicitly by an appropriate choice of P . The exact relationships
663 between, say, bed topography and P need to be mapped out experimentally (e.g., Inoue et al., 2014),
664 with theoretical approaches also providing some direction (cf. Johnson, 2014; Zhang et al., 2015).
665 Currently available experimental results (Chatanantavet and Parker, 2008; Finnegan et al., 2007;
666 Hodge and Hoey, 2016; Inoue et al., 2014; Johnson and Whipple, 2007) cover only a small range of
667 the possible parameter space and do not generally report all necessary parameters. Specifically the
668 stationary mass of sediment residing on the bed is generally not reported and can be difficult to
669 determine experimentally, but is necessary to determine P . Nevertheless, depending on the choice
670 of P , our model can yield a wide range of cover functions that encompasses reported functions both
671 from numerical modelling (e.g., Aubert et al., 2016; Hodge and Hoey, 2012; Johnson, 2014) and
672 experiments (Chatanantavet and Parker, 2008; Inoue et al., 2014; Sklar and Dietrich, 2001).

672



673 The dynamic model put forward here is a minimum first order formulation, and there are some
674 obvious future alterations. We only take account of the static cover effect caused by immobile
675 sediment on the bed. The dynamic cover effect, which arises when moving grains interact at high
676 sediment concentration and thus reduce the number of impacts on the bed (Turowski et al., 2007),
677 could in principle be included into the formulation, but would necessitate a second probability
678 function specifically to describe this dynamics cover. It would also be possible to use different P -
679 functions for entrainment and deposition, thus introducing hysteresis into cover development. Such
680 hysteresis has been observed in experiments in which the equilibrium sediment cover was a function
681 of the initial extent of sediment cover (Chatanantavet and Parker, 2008; Hodge and Hoey, 2012).
682 Whether such alterations are necessary is best established with targeted laboratory experiments.

683

684 **4.2 Comparison to previous modelling frameworks**

685 We will briefly outline in this section the main differences to previous formulations of cover dynamics
686 in bedrock channels. Thus, the novel aspects of our formulation and the respective advantages and
687 disadvantages will become clear.

688

689 Aubert et al. (2015) coupled the movement of spherical particles to the simulation of a turbulent
690 fluid and investigated how cover depended on transport capacity and supply. Similar to what is
691 predicted by our analytical formulation, they found a range of cover function for various model set-
692 ups, including linear and convex-up relationships (compare the results in Fig. 4 to their Fig. 15).
693 Despite short-comings, Aubert et al. (2015) presented the so far most detailed physical simulations of
694 bed cover formation and the correspondence between the predictions is encouraging.

695

696 Nelson and Seminara (2011, 2011) formulated a morphodynamic model for bedrock channels. They
697 based their formulation on sediment concentration, which is in principle similar to our formulation
698 based on mass. However, Nelson and Seminara (2011, 2012) did not distinguish between mobile and
699 stationary sediment and linked local transport directly to sediment concentration. Further, a given
700 mass can be distributed in multiple ways to achieve various degrees of cover, a fact that is quantified
701 in our formulation by the probability parameter P . Nelson and Seminara (2011, 2012) assumed a
702 direct correspondence between sediment concentration and degree of cover, which is equivalent to
703 the linear cover assumption (eq. 7), with the associated problems outlined earlier. Practically, this
704 implies that the grid size needs to be of the order of the grain size. Although different in various
705 details, Inoue et al. (2016) have used essentially the same approach as Nelson and Seminar (2011,
706 2012) to link bedload concentration, transport and bed cover. Both of these models allow the 2D
707 modelling of bedrock channel morphology. Although we have not fully developed such a model in
708 the present paper, our model framework could easily be extended to 2D problems.

709

710 Zhang et al. (2015) formulated a bed cover model specifically for beds with macro-roughness. There,
711 deposited sediment always fills topographic lows from their deepest positions, such that there is a
712 reach-uniform sediment level. While the model is interesting and provides a fundamentally different
713 approach to what is suggested here, its applicability is limited to very rough beds and the assumption
714 of a sediment elevation that is independent of the position on the bed seems physically unrealistic. In
715 principle, the probabilistic framework presented here should be able to deal with macro-rough beds
716 as well and thus allows a more general treatment of the problem of bed cover.

717

718 Within this paper, we focused on the dynamics of bed cover, rather than modelling the dynamics of
719 entire channels. The probabilistic formulation using the parameter P provides a flexible framework
720 to connect the sediment mass residing on the bed with the exposed bedrock fraction. This particular



721 element has not been treated in any of the previous models and could be easily implemented in
722 other approaches dealing with sediment fluxes along and across the stream and the interaction with
723 erosion and, over long time scales, channel morphology. However, it is as yet unclear how flow
724 hydraulics, sediment properties and other conditions affect P and this should be investigated in
725 targeted laboratory experiments. Nevertheless, the proposed formulation provides a framework in
726 which data from various sources can be easily compared and discussed.

727 728 **4.3 Further implications**

729 Based on field data interpretation, Phillips and Jerolmack (2016) argued that bedrock rivers adjust
730 such that, similar to alluvial channels, medium sized floods are most effective in transporting
731 sediment, and that channel geometry therefore can quickly adjust their transport capacity to the
732 applied load and therefore achieve grade (cf. Mackin, 1948). Contrary to the suggestion of Phillips
733 and Jerolmack (2016) that this is achieved by changing channel morphologic parameters such as
734 width, our model suggests that bed cover is adjusted. Furthermore changes in sediment cover can
735 occur far more rapidly than morphological changes. In steady state, time derivatives need to be equal
736 to zero to be equal to zero. Thus, entrainment equals deposition (eq. 16), implying that the
737 downstream gradient in sediment transport rate is equal to zero (eq. 14). When sediment supply or
738 transport capacity change, the exposed bedrock fraction can adjust to achieve a new steady state
739 and a change of the channel geometry is unnecessary. Whether a steady state is achieved depends
740 on the relative magnitude of the timescales of perturbation and cover adjustment (see section 3.2).

741

742 **5. Conclusions**

743

744 The probabilistic view put forward in this paper offers a framework into which diverse data on bed
745 cover, whether obtained from field studies, laboratory experiments or numerical modeling, can be
746 easily converted to be meaningfully compared. The conversion requires knowledge of the mass of
747 sediment on the bed and the evolution of exposed fraction of the bed. Within the framework,
748 individual data sets can be compared to the exponential benchmark and linear limit cases, enabling
749 physical interpretation. Furthermore, the formulation allows the general dynamic sub-grid modelling
750 of bed cover. Depending on the choice of P , the model yields a wide range of possible cover
751 functions. Which of these functions are appropriate for natural rivers and how they vary with factors
752 including topography needs to be mapped out experimentally.

753

754 It needs to be noted here that the precise formulation of the entrainment and deposition functions
755 also affects steady state cover relations. When calibrating P on data, it cannot always be decided
756 whether a specific deviation from the benchmark case results from varying entrainment and
757 deposition processes or from changes in the probability function driven for example by variations in
758 roughness. For the prediction of the steady state cover relations and for the comparison of data sets,
759 this should not matter, but the dynamic evolution of cover could be strongly affected.

760

761 The system timescale for cover adjustment is inversely related to transport capacity. This time scale
762 can be long and in many realistic situations, cover cannot instantaneously adjust to changes in the
763 forcing conditions. Thus, dynamic cover adjustment needs to be taken into account when modelling
764 the long-term evolution of bedrock channels.

765

766 Our model formulation implies that bedrock channels adjust bed cover to achieve grade. Therefore,
767 bedrock channel evolution is driven by two optimization principles. On short time scales, bed cover



768 adjusts to match the sediment output of a reach to its input. Over long time scales, width and slope
769 of the channel evolve to match long-term incision rate to tectonic uplift or base level lowering rates.
770



771 **Appendix A: Perturbation analysis**

772

773 Here, we derive the effect of a small sinusoidal perturbation of the driving variables, namely
 774 sediment supply q_s^* and transport capacity q_t^* , on cover development. The perturbation of the
 775 driving variables can be written as

776
$$q_s^* = \bar{q}_s^* + \delta q_s^*$$

777 (eq. A1)

778
$$q_t^* = \bar{q}_t^* + \delta q_t^*$$

779 (eq. A2)

780 Here, the bar denotes the average of the quantity at steady state, while δq_s^* and δq_t^* denote the
 781 small perturbation. The exposed area can be similarly written as

782
$$A^* = \bar{A}^* + \delta A^*$$

783 (eq. A3)

784 Steady state cover is directly related to the mass on the bed M_s^* by eq. (3), which we can rewrite as

785
$$\frac{dA^*}{dt} = -P \frac{dM_s^*}{dt}$$

786 (eq. A4)

787 Substituting eq. (A3) and a similar equation for M_s^* ,

788
$$M_s^* = \bar{M}_s^* + \delta M_s^*$$

789 (eq. A5)

790 we obtain

791
$$\frac{d\delta A^*}{dt} = -P \frac{d\delta M_s^*}{dt}$$

792 (eq. A6)

793 Here, the averaged terms drop out as they are independent of time. If P and the steady state
 794 solution for A^* are known, a direct relationship between A^* and M_s^* can be derived. For example, for
 795 the exponential cover model (eq. 2), substituting eqs. (A3) and (A5), we find

796
$$\bar{A}^* + \delta A^* = e^{-\bar{M}_s^* - \delta M_s^*} = e^{-\bar{M}_s^*} e^{-\delta M_s^*} = \bar{A}^* e^{-\delta M_s^*} \approx \bar{A}^* (1 - \delta M_s^*)$$

797 (eq. A7)

798 Here, since the δ variables are small, we approximated the exponential term using a Taylor expansion
 799 to first order. We obtain

800
$$\delta A^* = -\bar{A}^* \delta M_s^*$$

801 (eq. A8)

802 It is therefore sufficient to derive the perturbation solution for M_s^* , the time evolution of which is
 803 given by eq. (22). Eliminating M_m^* using eq. (24), we obtain

804
$$\frac{\partial M_s^*}{\partial t^*} = \left(1 - e^{-q_s^*/U^*}\right) q_s^* - \left(1 - e^{-M_s^*}\right) q_t^*$$

805 (eq. A9)

806

807 **Perturbation of sediment supply**

808

809 First, let's look at a perturbation of sediment supply q_s^* , while other parameters are held constant.

810 Substituting eq. (A1) and (A5) into (A9), we obtain

811
$$\frac{\partial \delta M_s^*}{\partial t^*} = \left(1 - e^{-(\bar{q}_s^* + \delta q_s^*)/U^*}\right) (\bar{q}_s^* + \delta q_s^*) - \left(1 - e^{-\bar{M}_s^* - \delta M_s^*}\right) q_t^*$$

812 (eq. A10)

813 Again, since the δ variables are small, we can replace the relevant exponentials with Taylor expansion
 814 to first order:



815
$$e^{-\delta q_s^*/U^*} \approx 1 - \frac{\delta q_s^*}{U^*}$$

816 (eq. A11)

817 A similar approximation applies for the exponential in M_s^* . Substituting eq. (A11) into eq. (A10),
 818 expanding the multiplicative terms, dropping terms of second order in the δ variables and
 819 rearranging, we get

820
$$\frac{\partial \delta M_s^*}{\partial t^*} = \delta q_s^* \left(1 - e^{-\bar{q}_s^*/U^*} + \frac{\bar{q}_s^*}{U^*} e^{-\bar{q}_s^*/U^*} \right) - \delta M_s^* \left(q_t^* - \left(1 - e^{-\bar{q}_s^*/U^*} \right) \bar{q}_s^* \right)$$

821 (eq. A12)

822 The perturbation is assumed to be sinusoidal

823
$$\delta q_s^* = d \sin\left(\frac{2\pi t}{p}\right)$$

824 (eq. A13)

825 Here, p is the period of the perturbation and d is its amplitude. Note that, to be consistent with the
 826 assumptions previously made, d needs to be small in comparison with the average sediment supply.
 827 Substituting, eq. (A12) can be integrated to obtain the solution

828
$$\delta M_s^* = G_{q_s^*} \sin\left(\frac{2\pi t}{p} + \varphi_{q_s^*}\right) + C \exp\left\{-\left(q_t^* - \left(1 - e^{-\bar{q}_s^*/U^*}\right) \bar{q}_s^*\right) \frac{t}{T}\right\}$$

829 where C is a constant of integration. The gain is given by

830
$$G_{q_s^*} = \frac{p}{T} \frac{\left(1 - e^{-\bar{q}_s^*/U^*} + \frac{\bar{q}_s^*}{U^*} e^{-\bar{q}_s^*/U^*}\right) d}{\sqrt{\left(q_t^* - \left(1 - e^{-\bar{q}_s^*/U^*}\right) \bar{q}_s^*\right)^2 \left(\frac{p}{T}\right)^2 + 4\pi^2}}$$

831 (eq. A14)

832 And the phase shift by

833
$$\varphi_{q_s^*} = \tan^{-1} \left[-\frac{2\pi}{\frac{p}{T} \left(q_t^* - \left(1 - e^{-\bar{q}_s^*/U^*}\right) \bar{q}_s^*\right)} \right]$$

834 (eq. A15)

835

836 Perturbation of transport capacity

837

838 The perturbation of the transport capacity q_i^* is a little more complicated, since both q_i^* and U^* are
 839 explicitly dependent on hydraulics (e.g., shear stress; see eqs. 43 and 44), and thus U^* is implicitly
 840 dependent on q_i^* and δq_i^* . To circumvent this problem, we expand the exponential term featuring
 841 $U^*(\delta q_i^*)$ in eq. (A9) using a Taylor series expansion around $\delta q_i^* = 0$.

842

843
$$\exp\left\{-\frac{q_s^*}{U^*(\delta q_t^*)}\right\} \approx \exp\left\{-\frac{q_s^*}{U^*(\delta q_t^* = 0)}\right\} \left[1 - \frac{q_s^*}{U^{*2}(\delta q_t^* = 0)} \frac{\partial U^*}{\partial \delta q_t^*}(\delta q_t^* = 0) \delta q_t^* \right]$$

844 (eq. A16)

845 Both U^* and its derivative are constants when evaluated at $\delta q_i^* = 0$. We can thus write

846

847
$$\exp\left\{-\frac{q_s^*}{U^*}\right\} = \exp\left\{-\frac{q_s^*}{U^*}\right\} \left[1 - \frac{q_s^*}{U^{*2}} \left(\frac{\partial U^*}{\partial \delta q_t^*}\right) \delta q_t^* \right] = [1 - C_0 \delta q_t^*] e^{-q_s^*/U^*}$$

848

849 (eq. A17)



850 Here, C_0 is a constant. Proceeding as before by substituting eq. (A2), (A8) and (A17) into (A9),
 851 expanding exponential terms containing δ variables, dropping terms of second order in the δ
 852 variables and rearranging, we obtain:

$$853 \quad \frac{\partial \delta M_s^*}{\partial t^*} = \left(B q_s^* e^{-q_s^*/\bar{U}^*} + e^{-\bar{M}_s^*} - 1 \right) \delta q_t^* - \delta M_s^* \bar{q}_t^* e^{-\bar{M}_s^*}$$

854 (eq. A18)

855 A sinusoidal perturbation of the form

$$856 \quad \delta q_t^* = d \sin\left(\frac{2\pi t}{p}\right)$$

857 (eq. A19)

858 yields the solution

$$859 \quad \delta M_s^* = G_{q_t^*} \sin\left(\frac{2\pi t}{p} + \varphi_{q_t^*}\right) + C \exp\left\{-\left(\bar{q}_t^* - \left(1 - e^{-q_s^*/\bar{U}^*}\right) q_s^*\right) \frac{t}{p}\right\} \left\{-\left(\bar{q}_t^* - \left(1 - e^{-q_s^*/\bar{U}^*}\right) q_s^*\right) \frac{t}{T}\right\}$$

860 with

$$861 \quad G_{q_t^*} = \frac{p \left(\frac{q_s^{*2}}{\bar{U}^{*2}} \left(\frac{\partial U^*}{\partial \delta q_t^*} \right) e^{-q_s^*/\bar{U}^*} - \left(1 - e^{-q_s^*/\bar{U}^*}\right) \frac{q_s^*}{\bar{q}_t^*} \right) d}{\sqrt{\bar{q}_t^{*2} \left(\frac{p}{T}\right)^2 \left(1 - \left(1 - e^{-q_s^*/\bar{U}^*}\right) \frac{q_s^*}{\bar{q}_t^*}\right)^2 + 4\pi^2}}$$

862 (eq. A20)

863 and

$$864 \quad \varphi = \tan^{-1}\left(-\frac{2\pi}{\frac{p}{T} \left(\bar{q}_t^* - \left(1 - e^{-q_s^*/\bar{U}^*}\right) q_s^*\right)}\right)$$

865 (eq. A21)

866

867 Summary

868

869 Using the system timescale T_s , the phase shift and gain can be generally rewritten as

870

$$871 \quad \varphi = \tan^{-1}\left(-2\pi \frac{T_s}{p}\right)$$

872 (eq. A22)

$$873 \quad G = \frac{p}{T_s} \frac{Kd}{\sqrt{\left(\frac{p}{T_s}\right)^2 + 4\pi^2}}$$

874 (eq. A23)

875 Here, K differs for perturbations in sediment supply and transport capacity, given by the equations

876

$$877 \quad K_{q_s^*} = 1 - e^{-\bar{q}_s^*/U^*} + \frac{\bar{q}_s^*}{U^*} e^{-\bar{q}_s^*/U^*}$$

878 (eq. A24)

$$879 \quad K_{q_t^*} = \frac{q_s^{*2}}{\bar{U}^{*2}} \left(\frac{\partial U^*}{\partial \delta q_t^*} \right) e^{-q_s^*/\bar{U}^*} - \left(1 - e^{-q_s^*/\bar{U}^*}\right) \frac{q_s^*}{\bar{q}_t^*}$$

880 (eq. A25)

881

882



883 **Notation**

884

885 Overbars denote time-averaged quantities.

886

887 a Shape parameter in the regularized incomplete Beta function.

888 A^* Fraction of exposed (uncovered) bed area.

889 b Shape parameter in the regularized incomplete Beta function.

890 B Regularized incomplete Beta function.

891 C Constant of integration.

892 C_0 Constant [$\text{m}^2\text{s}/\text{kg}$].

893 d Amplitude of perturbation [$\text{kg}/\text{m}^2\text{s}$].

894 D Sediment deposition rate per bed area [$\text{kg}/\text{m}^2\text{s}$].

895 D^* Dimensionless sediment deposition rate.

896 D_{50} Median grain size [m].

897 e Base of the natural logarithm.

898 E Sediment entrainment rate per bed area [$\text{kg}/\text{m}^2\text{s}$].

899 E^* Dimensionless sediment entrainment rate.

900 E_{max} Maximal possible dimensionless sediment entrainment rate.

901 g Acceleration due to gravity [m/s^2].

902 G Gain [$\text{kg}/\text{m}^2\text{s}$].

903 I Non-dimensional incision rate.

904 k Probability of sediment deposition on uncovered parts of the bed, linear
905 implementation.

906 k_I Non-dimensional erodibility.

907 K Parameter in the gain equation.

908 L Characteristic length scale [m].

909 M_0 Minimum mass per area necessary to cover the bed [kg/m^2].

910 M_0^* Dimensionless characteristic sediment mass.

911 M_m Mobile sediment mass [kg/m^2].

912 M_m^* Dimensionless mobile sediment mass.

913 M_s Stationary sediment mass [kg/m^2].

914 M_s^* Dimensionless stationary sediment mass.

915 p Period of perturbation [s].

916 P Probability of sediment deposition on uncovered parts of the bed.

917 q_s Mass sediment transport rate per unit width [kg/ms].

918 q_s^* Dimensionless sediment transport rate.

919 q_t Mass sediment transport capacity per unit width [kg/ms].

920 q_t^* Dimensionless transport capacity.

921 Q_s^* Relative sediment supply; sediment transport rate over transport capacity.

922 Q_t Mass sediment transport capacity [kg/s].

923 t Time variable [s].

924 t^* Dimensionless time.

925 T Characteristic time scale [s].

926 T_E Characteristic time scale for sediment entrainment [s].

927 T_S Characteristic system time scale [s].

928 U Sediment speed [m/s].

929 U^* Dimensionless sediment speed.

930 x Dimensional streamwise spatial coordinate [m].



931	x^*	Dimensionless streamwise spatial coordinate.
932	y	Dummy variable.
933	α	Exponent.
934	γ	Fraction of pore space in the sediment.
935	δ	denotes time-varying component.
936	θ	Shields stress.
937	θ_c	Critical Shields stress.
938	ρ	Density of water [kg/m ³].
939	ρ_s	Density of sediment [kg/m ³].
940	τ	Bed shear stress [N/m ²].
941	τ_c	Critical bed shear stress at the onset of bedload motion [N/m ²].
942		
943		



944 **Acknowledgements**

945

946 We thank Joel Scheingross and Jean Braun for insightful discussions. The data from the Erlenbach is
947 owned by and is used with permission of the Mountain Hydrology and Mass Movements Group at
948 the Swiss Federal Research Institute for Forest Snow and Landscape Research WSL.

949

950 **References**

951

- 952 Aubert, G., V.J. Langlois, P. Allemand (2016). Bedrock incision by bedload: Insights from direct
953 numerical simulations. *Earth Surf. Dynam.*, 4, 327-342, doi: 10.5194/esurf-4-327-2016
- 954 Beer, A. R. & Turowski, J. M. (2015). Bedload transport controls bedrock erosion under sediment-
955 starved conditions. *Earth Surface Dynamics*, 3, 291-309, doi: 10.5194/esurf-3-291-2015
- 956 Beer, A.R., J.M. Turowski, B. Fritschi, D.H. Rieke-Zapp, (2015). Field instrumentation for high-
957 resolution parallel monitoring of bedrock erosion and bedload transport, *Earth Surface*
958 *Processes and Landforms*, 40, 530-541, doi: 10.1002/esp.3652
- 959 Charru, F.; Mouilleron, H. & Eiff, O. (2004). Erosion and deposition of particles on a bed sheared by a
960 viscous flow. *J. Fluid Mech.*, 519, 55-80
- 961 Chatanantavet, P. & Parker, G. (2008). Experimental study of bedrock channel alluviation under
962 varied sediment supply and hydraulic conditions. *Water Resour. Res.*, 44, W12446, doi:
963 10.1029/2007WR006581
- 964 Cook, K.; Turowski, J. M. & Hovius, N. (2013). A demonstration of the importance of bedload
965 transport for fluvial bedrock erosion and knickpoint propagation. *Earth Surf. Process.*
966 *Landforms*, 38, 683-695, doi: 10.1002/esp.3313
- 967 Fernandez Luque, R. & van Beek, R. (1976). Erosion and transport of bed-load sediment. *J. Hydraul.*
968 *Res.*, 14, 127-144
- 969 Finnegan, N. J.; Sklar, L. S. & Fuller, T. K. (2007). Interplay of sediment supply, river incision, and
970 channel morphology revealed by the transient evolution of an experimental bedrock channel.
971 *Journal of Geophysical Research*, 112, F03S11, doi: 10.1029/2006JF000569
- 972 Gilbert, G. K. (1877), Report on the geology of the Henry Mountains: Geographical and geological
973 survey of the Rocky Mountain region, U.S. Gov. Print. Off., Washington, D. C.
- 974 Hobley, D. E. J.; Sinclair, H. D.; Mudd, S. M. & Cowie, P. A. (2011). Field calibration of sediment flux
975 dependent river incision. *J. Geophys. Res.*, 116, F04017, doi: 10.1029/2010JF001935
- 976 Hodge, R.A. (in press) Sediment processes in bedrock-alluvial rivers: Research since 2010 and
977 modelling the impact of fluctuating sediment supply on sediment cover. In: Tsutsumi, D. &
978 Laronne, J. *Gravel-Bed Rivers: Process and Disasters*. Wiley-Blackwell.
- 979 Hodge, R. A. & Hoey, T. B. (2012). Upscaling from grain-scale processes to alluviation in bedrock
980 channels using a cellular automaton model. *J. Geophys. Res.*, 117, F01017, doi:
981 10.1029/2011JF002145
- 982 Hodge, R. A., T. B. Hoey, and L. S. Sklar (2011), Bedload transport in bedrock rivers: the role of
983 sediment cover in grain entrainment, translation and deposition, *J. Geophys. Res.*, 116,
984 F04028, doi: 10.1029/2011JF002032.
- 985 Hodge, R. A., and T. B. Hoey (2016), A Froude scale model of a bedrock-alluvial channel reach: 2.
986 Sediment cover, *J. Geophys. Res.*, in press, doi: 10.1002/2015JF003709
- 987 Inoue, T., N. Izumi, Y. Shimizu, G. Parker (2014). Interaction among alluvial cover, bed roughness, and
988 incision rate in purely bedrock and alluvial-bedrock channel. *J. Geophys. Res.*, 119, 2123-
989 2146, doi: 10.1002/2014JF003133



- 990 Inoue, T., T. Iwasaki, G. Parker, Y. Shimizu, N. Izumi, C.P. Stark, J. Funaki (2016). Numerical simulation
991 of effects of sediment supply on bedrock channel morphology. *J. Hydr. Eng.*, in press, doi:
992 10.1061/(ASCE)HY.1943-7900.0001124
- 993 Johnson, J.P.L. (2014). A surface roughness model for predicting alluvial cover and bed load transport
994 rate in bedrock channels. *J. Geophys. Res.*, 119, 2147-2173, doi: 10.1002/2013JF003000
- 995 Johnson, J. P. & Whipple, K. X. (2007). Feedbacks between erosion and sediment transport in
996 experimental bedrock channels. *Earth Surf. Process. Landforms*, 32, 1048-1062, doi:
997 10.1002/esp.1471
- 998 Lague, D. (2010), Reduction of long-term bedrock incision efficiency by short-term alluvial cover
999 intermittency, *J. Geophys. Res.*, 115, F02011, doi:10.1029/2008JF001210
- 1000 Lajeunesse, E.; Malverti, L. & Charru, F. (2010). Bed load transport in turbulent flow at the grain
1001 scale: Experiments and modeling. *Journal of Geophysical Research*, 115, F04001
- 1002 Paola, C. & Voller, V. R. (2005). A generalized Exner equation for sediment mass balance. *J. Geophys.*
1003 *Res.*, 110, F04014
- 1004 Phillips, C.B., D.J. Jerolmack (2016). Self-organization of river channels as a critical filter on climate
1005 signals. *Science*, 352, 694-697
- 1006 Mackin JH. (1948). Concept of the graded river. *Geological Society of America Bulletin* 59: 463-512.
1007 doi: 10.1130/0016-7606(1948)59[463:COTGR]2.0.CO;2
- 1008 Meyer-Peter, E., and R. Mueller (1948), Formulas for bedload transport, in 2nd meeting Int. Assoc.
1009 Hydraulic Structures Res., edited, Stockholm, Sweden.
- 1010 Molnar P, Densmore AL, McCardell BW, Turowski JM, Burlando P. (2010). Analysis of changes in the
1011 step-pool morphology and channel profile of a steep mountain stream following a large
1012 flood. *Geomorphology* 124: 85–94. DOI. 10.1016/j.geomorph.2010.08.014
- 1013 Nelson, P. A., and G. Seminara (2011), Modeling the evolution of bedrock channel shape with erosion
1014 from saltating bed load, *Geophys. Res. Lett.*, 38, L17406, doi: 10.1029/2011GL048628
- 1015 Nelson, P. A., and G. Seminara (2012), A theoretical framework for the morphodynamics of bedrock
1016 channels, *Geophys. Res. Lett.*, 39, L06408, doi: 10.1029/2011GL050806.
- 1017 Nitsche, M., D. Rickenmann, J.M. Turowski, A. Badoux, J.W. Kirchner, (2011). Evaluation of bedload
1018 transport predictions using flow resistance equations to account for macro-roughness in
1019 steep mountain streams, *Water Resources Research*, 47, W08513, doi:
1020 10.1029/2011WR010645
- 1021 Rickenmann D, Turowski JM, Fritschi B, Klaiiber A, Ludwig A. (2012). Improved sediment transport
1022 measurements in the Erlenbach stream including a moving basket system. *Earth Surface*
1023 *Processes and Landforms* 37: 1000–1011, doi: 10.1002/esp.3225
- 1024 Sklar, L. S. & Dietrich, W. (1998). River longitudinal profiles and bedrock incision models: Stream
1025 power and the influence of sediment supply. In: *Rivers over Rock: Fluvial Processes in*
1026 *Bedrock Channels*, E. Tinkler, K. J. & Wohl, E. E. (Eds.), American Geophysical Union, 107, 237-
1027 260
- 1028 Sklar, L.S., Dietrich, W.E., (2001). Sediment and rock strength controls on river incision into bedrock.
1029 *Geology* 29, 1087-1090, doi: 10.1130/0091-7613(2001)029<1087:SARSCO>2.0.CO;2
- 1030 Sklar, L. S. & Dietrich, W. E. (2004). A mechanistic model for river incision into bedrock by saltating
1031 bed load. *Water Resour. Res.*, 40, W06301, doi: 10.1029/2003WR002496
- 1032 Turowski, J. M. (2009). Stochastic modeling of the cover effect and bedrock erosion. *Water Resour.*
1033 *Res.*, 45, W03422, doi: 10.1029/2008WR007262
- 1034 Turowski, J. M. & Bloem, J.-P. (2016). The influence of sediment thickness on energy delivery to the
1035 bed by bedload impacts. *Geodinamica Acta*, 28, 199-208, doi:
1036 10.1080/09853111.2015.1047195



- 1037 Turowski, J. M. & Rickenmann, D. (2009). Tools and cover effects in bedload transport observations
1038 in the Pitzbach, Austria. *Earth Surf. Process. Landforms*, 34, 26-37, doi: 10.1002/esp.1686
- 1039 Turowski, J. M.; Lague, D. & Hovius, N. (2007). Cover effect in bedrock abrasion: A new derivation
1040 and its implication for the modeling of bedrock channel morphology *J. Geophys. Res.*, 112,
1041 F04006, doi: 10.1029/2006JF000697
- 1042 Turowski, J. M.; Hovius, N.; Hsieh, M.-L.; Lague, D. & Chen, M.-C. (2008). Distribution of erosion
1043 across bedrock channels. *Earth Surf. Process. Landforms*, 33, 353-363, doi: 10.1002/esp.1559
- 1044 Turowski JM, Yager EM, Badoux A, Rickenmann D, Molnar P. (2009). The impact of exceptional
1045 events on erosion, bedload transport and channel stability in a step-pool channel. *Earth*
1046 *Surface Processes and Landforms* 34: 1661–1673, doi: 10.1002/esp.1855
- 1047 Wohl, E. E. & Ikeda, H. (1997). Experimental simulation of channel incision into a cohesive substrate
1048 at varying gradients. *Geology*, 25, 295-298, doi: 10.1130/0091-
1049 7613(1997)025<0295:ESOCII>2.3.CO;2
- 1050 Wyss, C.R., D. Rickenmann, B. Fritschi, J.M. Turowski, V. Weitbrecht, R.M. Boes, (2016). Measuring
1051 bedload transport rates by grain-size fraction using the Swiss Plate Geophone signal at the
1052 Erlenbach, *Journal of Hydraulic Engineering*, 142(5), 04016003, doi: 10.1061/(ASCE)HY.1943-
1053 7900.0001090
- 1054 Yanites, B. J.; Tucker, G. E.; Hsu, H.-L.; Chen, C.-C.; Chen, Y.-G. & Mueller, K. J. (2011). The influence of
1055 sediment cover variability on long-term river incision rates: An example from the Peikang
1056 River, central Taiwan. *J. Geophys. Res.*, 116, F03016, doi: 10.1029/2010JF001933
- 1057 Zhang, L., G. Parker, C.P. Stark, T. Inoue, E. Viparelli, X. Fu, N. Izumi (2015). Macro-roughness model
1058 of bedrock-alluvial river morphodynamics. *Earth Surface Dynamics*, 3, 113-138, doi:
1059 10.5194/esurf-3-113-2015
- 1060